CONTRACTOR REPORT

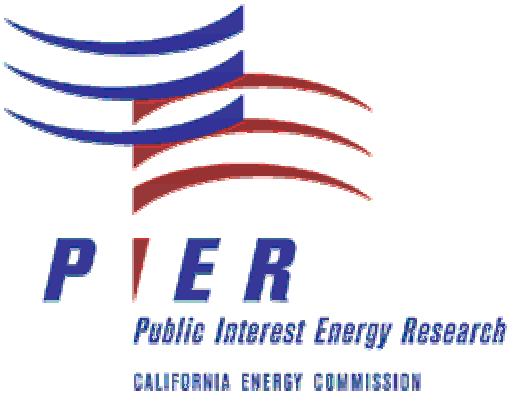

Environmentally-Preferred Advanced Generation

Durability of Catalytic Combustion Systems

APPENDIX III: Combustion Catalyst Axial Support Mechanical Durability

Gray Davis, *Governor*

January 2002

CALIFORNIA ENERGY COMMISSION

RESOURCES AGENCY

CALIFORNIA ENERGY COMMISSION

Prepared for:

CALIFORNIA ENERGY COMMISSION

Avtar Bining, *Contract Manager*
ENGINEERING OFFICE

Mike Batham, *Program Lead*
Environmentally-Preferred Advanced Generation

Prepared by:
John Barnes
Marco Velasco
Jim Schlatter

CATALYTICA ENERGY SYSTEMS
Mountain View, CA

Contract No. 500-97-033

Contract Amount: $1,316,030

Legal Notice

Table of Contents

List of Figures

Figure **Page**

List of Tables

Preface

The Public Interest Energy Research (PIER) Program supports public interest energy research and development that will help improve the quality of life in California by bringing environmentally safe, affordable, and reliable energy services and products to the marketplace.

The PIER Program, managed by the California Energy Commission (Commission), annually awards up to $62 million to conduct the most promising public interest energy research by partnering with Research, Development, and Demonstration (RD&D) organizations, including individuals, businesses, utilities, and public or private research institutions.

PIER funding efforts are focused on the following six RD&D program areas:

- Buildings End-Use Energy Efficiency
- Industrial/Agricultural/Water End-Use Energy Efficiency
- Renewable Energy
- Environmentally-Preferred Advanced Generation
- Energy-Related Environmental Research
- Strategic Energy Research.

What follows is the topical report for the Durability of Catalytic Combustion Systems Project, conducted by Catalytica Energy Systems. The report is entitled "**Combustion Catalyst Axial Support Mechanical Durability".** This project contributes to the Environmentally-Preferred Advanced Generation program.

For more information on the PIER Program, please visit the Commission's Web site at: http://www.energy.ca.gov/research/index.html or contact the Commission's Publications Unit at 916-654-5200.

I. Introduction

This report describes work completed to predict the mechanical durability of the catalyst axial support referred to as the bonded metal monolith (BMM). This component is critical to the operation of the gas turbine combustion system and must survive over 8000 hours at high temperature and constant mechanical load. Limited operating experience exists for this unique application creating a need to develop a methodology for predicting and designing for long-term durability.

The function of the axial support is to restrain the catalyst foils from movement due to the force of the combustion gas flow. The contact pressure against the catalyst foils must be sufficiently low to avoid locally deforming the foils. Since the restraint must occur at the exit of the combustion gas from the catalyst, the axial support operates at very high temperature. Also, minimal airflow must be blocked to avoid flow disturbances. To accomplish these objectives, a high temperature alloy foil honeycomb is employed which distributes the contact to many contact areas while providing very low flow blockage.

Durability issues for the axial support are the typical failure mechanisms considered in gas turbine hot section design: permanent deformation due to creep and plasticity and low cycle fatigue due to thermal and mechanical loading. Oxidation is also a durability concern, but will not be discussed here.

II. Approach

As is common in gas turbine component design, a combination of structural analysis and material testing was selected as the best method for determining the durability of the BMM. Although proving long-term durability using the actual component at turbine operating conditions would be the most convincing approach, it was not deemed practical for several reasons. First, the temperature distribution and pressure loading were found to be very difficult to reproduce in a test configuration. Second, because the length of time required for the test was greater than 8000 hours, the commitment of facilities and personnel was excessive. Acceleration of the durability test was considered but found to add too much uncertainty to the results.

Another equally important reason for not relying on component durability testing is the lack of insight gained --- the component would reveal little information regarding the cause of the final condition. In particular, plasticity, creep or cyclic ratcheting could cause excessive deformation but which was predominant would not be revealed. The relative effect of the thermal loading versus the pressure loading would also not be determined. In addition, how close the component is to the durability limit or how much additional loading can be tolerated would not be quantified from a single component test.

Material specimen testing had to be included in the program since very little data was available. The published data was reviewed and utilized when possible but did not adequately represent the honeycomb. In particular, it is believed that the properties are affected by the thinness of the foil along with the brazing and pretreatment processes.

Finite element analyses were needed for the structural computations due to the complex geometry and thermal loading. The stress distribution within the honeycomb has very large variation due to the curvature and the braze joints in the honeycomb. The peak stress concentrations must be

accurately computed to determine fatigue life. Permanent deformation is dictated by the summation of plastic and creep strain throughout the honeycomb material so a precise calculation of the stress distribution is needed. Material properties were fit to analytical models for input into the finite element analyses.

III. Material Property Data

3.1 Measurement of Material Properties

The current base material for the BMM is Haynes 214 (designated H214 hereinafter), a high temperature NiCrAl superalloy. Limited materials properties for this alloy were published in the brochure provided by Haynes. However, this information is typically averaged data and may not be representative of the thin foil used in the honeycomb. In addition, the BMM uses a brazed, pretreated, and heat-treated material that may have significantly different properties from the base material. [The details of the pretreatment are proprietary and are not included in this report.] Therefore, it was deemed critical to obtain detailed material properties for foil that had been exposed to the braze cycle and to the intended other treatments.

The elastic plastic, fatigue, and creep testing was completed for the material treatments listed in Table 3.1.1:

Material	Elastic-plastic	Creep	Fatigue
Base case	X		X
Heat treated	X		
Pretreated	X	X	X
Pretreated and brazed	X	X	

Table 3.1.1 -- Haynes 214 Treatments for Testing

The creep tests were done with two similar pretreated materials, one that had been through the brazing cycle and one that had not. The objective was to test the pretreated H214 for at least 4000 to 8000 hours, while the brazed counterpart would only be run for a shorter duration of 2000 hours. The short duration would provide adequate evidence if the two materials are significantly different.

The “Base case” indicates testing an as-received H214 foil from Haynes and exposing it to a brazing thermal cycle without any actual brazing. The “Heat treated” designation indicates having a pretreatment in 1-atm air at 1920°F (1050°C) for 10 hours, thus ensuring the formation of a protective alumina layer. “Pretreated” indicates addition of an extra pretreatment step in the H214 processing. Finally, the “Pretreated and brazed” sample had two foils brazed together along their center-span.

The elastic-plastic tests and creep were done with a 0.010-inch thick foil, while the fatigue testing was done on a 0.090-inch thick sheet. The increase in thickness for the fatigue testing was necessary to prevent buckling when the specimen is compressed after tensile yielding at the high strain needed to cause fatigue.

3.2 Creep Testing of Foils

Due to a limited number of machines for creep testing, only the pretreated H214 was tested at stresses of 500 and 1000 psi, with each stress at 1562°F (850°C), 1652°F (900°C), and 1742°F (950 °C).

As the testing progressed, it became apparent that the creep rates of several of the samples were inconsistent (see Figures A1 to A3 in Appendix A). All the samples, with the exception of two (1562°F/1000 psi and 1652°F/1000psi), appeared to be elongating normally. The "normal" samples had the classic primary creep portion, along with the more stable secondary creep portion. The two "abnormal" samples exhibited elongation rates higher than the rest of the samples, so these tests were stopped due to the possibility of defects in either the sample material itself or experimental set-up error. The two samples were then re-tested which produced similarly inconsistent results.

After careful evaluation and inspection of the equipment and in-progress results, it was determined that the thin foils combined with the extensometer were causing the unexpected results. The extensometer is an instrument commonly used for measuring minute deformations in both elevated temperature tensile and creep tests. The following observations lead to the explanation of the test inconsistency:

- The loading needed in the creep test to obtain axial stress of 500 and 1000 psi in these thin specimens (.010 inch) is very small. Consequently the extensometer and insulation friction and the linear variable displacement transducer (LVDT) spring rate may be significant compared to the loading. There may be stick -slip in the extensometer mechanism as well causing erratic loading. These factors cause under loading and intermittent loading of the specimen leading to <u>less than expected creep strain</u>.
- Using the Haynes published data, an upper limit on creep strain can be obtained. At 1800F, 960 psi is required to cause a creep strain of 1 % in 1000 hours. Several test points exceeded this value. Unfortunately, friction and stick- slip do not explain <u>higher than expected creep strain</u>.
- The three tests considered "normal" (1652°F/500 psi, 1742°F at 500 and 1000 psi), were producing very similar creep even though conditions are quite different.
    - Haynes data shows that small stress changes (870 to 960 psi) cause twice the creep strain (0.5 to 1.0%) at 1800°F, and similar response exists at 1600 and 1700°F. The Materials Characterization Labs (MCL) testing shows very similar strain for 500 and 1000 psi at 1742°F.
    - Haynes data also shows that 100F temperature increase produces the same creep strain if the stress is divided by approximately 3 (960 psi at 1800°F and 3100 psi at 1700°F and 6800 psi at 1600°F all cause 1.0% strain in 1000 hrs). The MCL testing shows similar results for 500 psi at 1652 and 1742°F.

Shortly after, all testing was stopped and the elongation checked manually. In all the samples with greater than 2500 hours, the elongation checked manually proved to have a higher creep

strain of twice to three times greater than the extensometer reading at the time the sample was stopped (the manually measured elongation is indicated by arrows in Figures A1 to A3). This was more evidence supporting that the extensometer was inadequate, and that the foils were creeping at much higher rates than expected.

At this point, there were several adjustments that could be made in future testing. The samples could be increased in thickness and/or width to increase the load relative to the extensometer, or the extensometer eliminated altogether. However, there is undocumented evidence that material with only 2 or 3 grains through the thickness can have significantly higher creep rates than thicker samples. This is caused by the relative freedom for the grains to shear. Previous examination of a service-exposed BMM showed 2 or 3 grains through the wall. Therefore, it was again decided that thickness could not be increased. The widest sample that MCL can accommodate on their creep machines is 0.4 inches at the gage section. This is an increase of 1.6 times the width from the current 0.25 inches. This higher width translates to an increase in load of 1.6 times which was not considered enough to overcome the stick-slip.

Eliminating the extensometer was the best option to remove the stick-slip unknown. The main drawback to this approach is that continuous points will not be obtained, and that the primary creep might be missed. Discrete points will be obtained by stopping to measure at selected intervals.

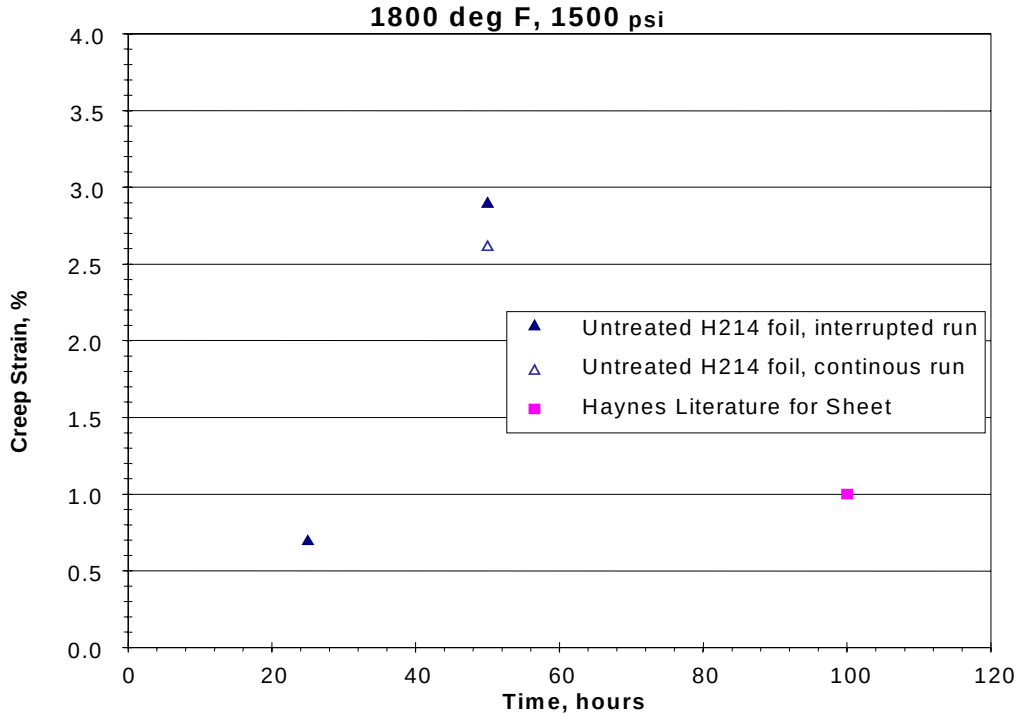

Figure 3.2.1 -- Comparison of the creep properties of foil versus sheet form at 1800F and 1500 psi

In order to validate the procedure without the extensometer, a short test of H214 foil was completed and compared to the manufacturer's sheet data (Appendix B). This test originally consisted of doing a 100-hour test at 1800F and 1500 psi of an untreated H214 foil, in order to try to match the creep of Haynes sheet (1.0%) without the extensometer. The first sample was

stopped and measured at 25 hours, and then at 50 hours (see the "interrupted run" in Figure 3.2.1 above). The results were surprising, showing a creep of 0.7% for the first 25 hours, and 2.9% after a total of 50 hours. Since the results had such an obvious increase in elongation when compared to the sheet form, it was decided that running to 100 hours was unnecessary. Instead, it was deemed more important to run another sample for a continuous 50 hours. There was some initial concern that the creep properties would have been altered due to the cool-down during measurements. The results of the second creep test helped to dispel this last concern, showing a creep of 2.62%. If the results from the two runs are averaged at 50 hours, its shows an average creep of 2.8%; 2.8 times that of the sheet form.

3.3 Fatigue Testing

The fatigue testing of H214 samples was done at Mar-Test (a division of MCL). Two variations of the same material were tested, an H214 sample exposed to the brazing cycle, and a pretreated H214. Each specimen has a thickness of 0.090 inches, and was run at 1562, 1650, 1740 and 1830°F (850, 900, 950, and 1000 °C). Three strain ranges per temperature, A Ratio = +1, two minute tensile hold were completed. Strain ranges were chosen to obtain failures between 100 and 1000 cycles.

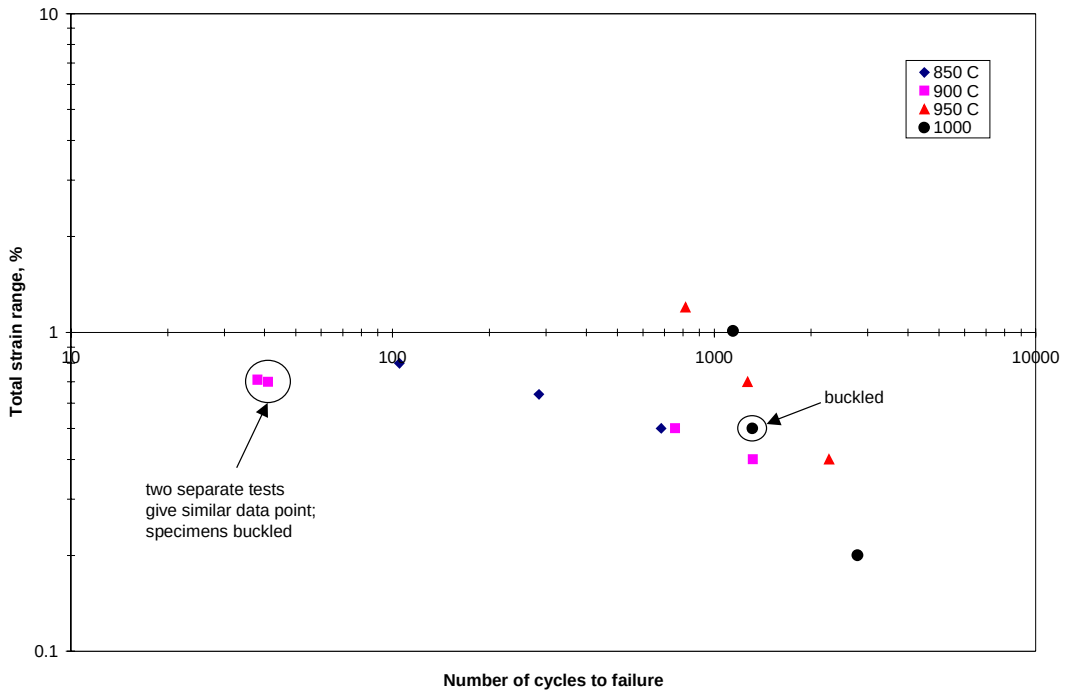

Figure 3.3.1 -- LCF results of H214 exposed to the braze cycle

Note that across every temperature, the pretreated H214 gives lower cycles to failure than the heat-treated H214. The best results for comparing the two types of materials were chosen at 850 and 950 °C (see Figure 3.3.3). Note that the pretreated material at 950 °C has its low-cycle fatigue curve almost on top of the heat-treated material at 850 °C. It is obvious that the fatigue

properties of H214 are reduced when it is pretreated. For example, at a strain range of 0.7%, the pretreated H214 has 127 cycles to failure, whereas the H214 that is exposed to the braze cycles has 1270 cycles to failure. However, as the strain range is reduced, the difference in cycles to failure between the pretreated and non-pretreated becomes smaller.

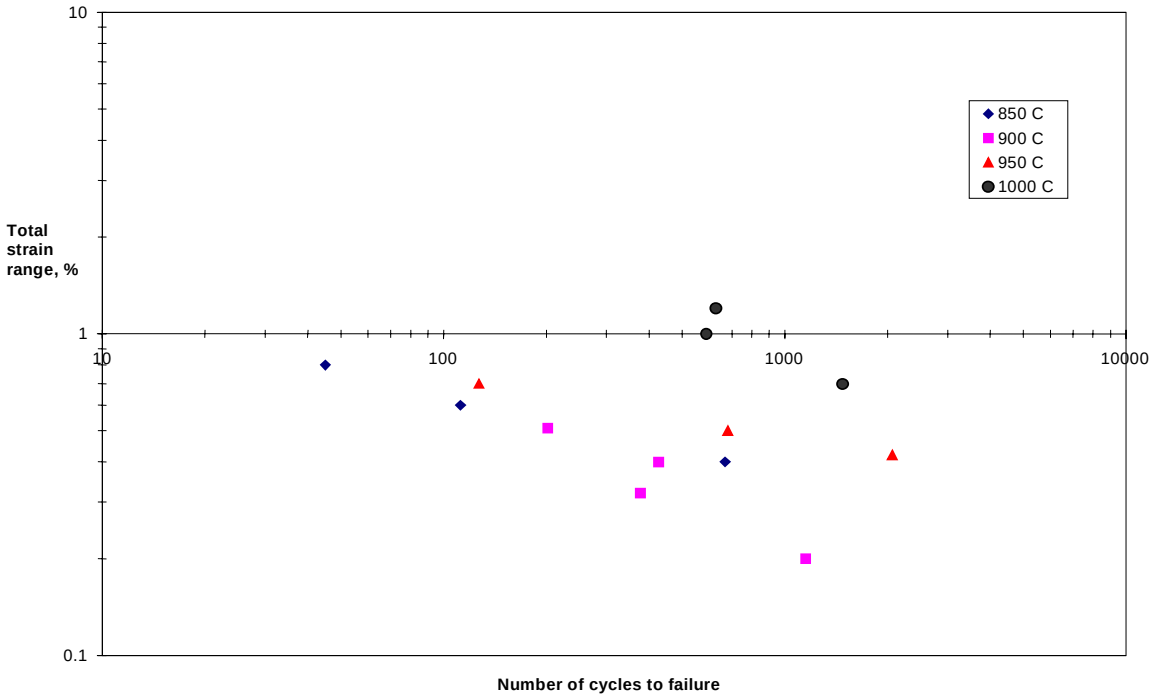

Figure 3.3.2 -- LCF test results of the pretreated H214

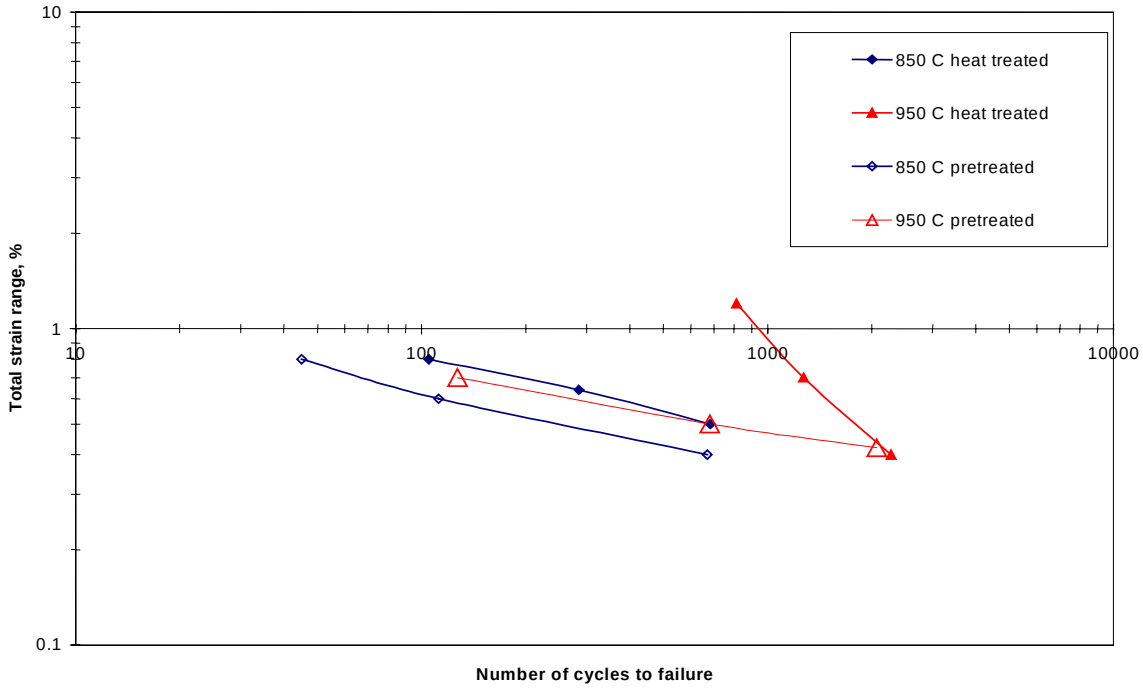

Figure 3.3.3 -- Comparison of LCF results for both materials at 850 and 950 ℃

3.4 Elastic-Plastic Testing

Four variations of the H214 foils were tested at MCL as shown below in Table 3.4.1.

Material	Material Designation
Base case (untreated) H214	1T
Heat treated H214	1BT
Pretreated H214	2T
Pretreated and brazed H214	3T

Table 3.4.1-- Fatigue testing matrix

Each material was run at 875, 925, and 975 °C, with three tests at each temperature.
Initial test results have been completed, but further tests will be needed to ensure data quality.
The results of the testing are shown below in Figures 3.4.1 and 3.4.2.

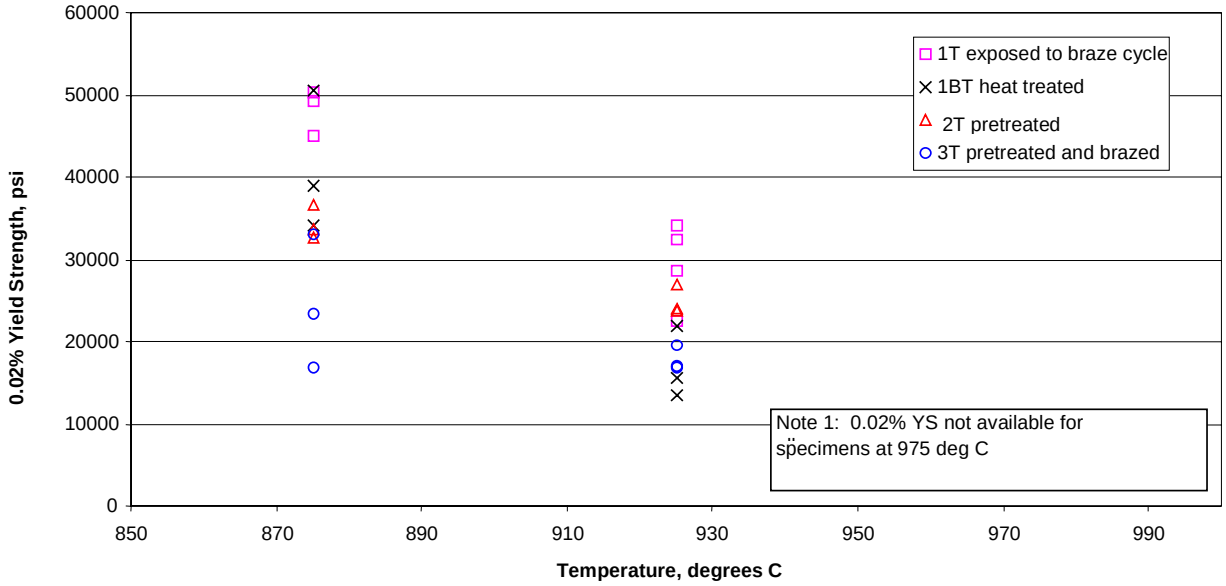

Figure 3.4.1 -- 0.02% Yield Strength versus Temperature

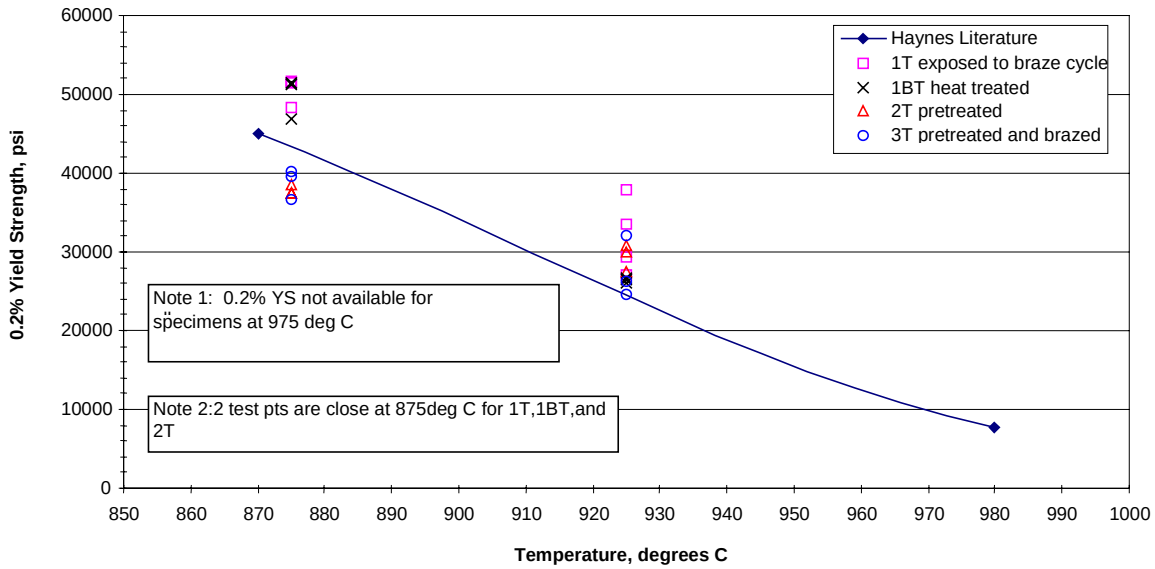

Figure 3.4.2 -- 0.2% Yield Strength versus Temperature

IV. Material Constitutive Model for Structural Analysis

4.1 Physical Properties

Temperature dependent material physical properties were obtained from the Haynes 214 brochure [see Appendix B] and are summarized in Table 4.1.1.

Physical Property	70°F	1000°F	1200°F	1400°F	1600°F	1700°F	1800°F	1850°F
Young's Modulus (Msi)	31.6	25.3	23.9	22.3	20.2	19.9	19	18.5
Poisson's Ratio	0.28	0.31	0.31	0.32	0.32	0.32	0.32	0.32
Coefficient of thermal expansion (10^{-6}in/in/°F)	7.4	8.2	8.6	9	9.6	9.9	10.2	10.4
Conductivity (BTU in/ft^2 hr °F)	83	153	175	200	215	225	227	227

Table 4.1.1 -- H214 Temperature Dependent Physical Properties

4.2 Plasticity

Plasticity was represented by temperature dependent multilinear kinematic hardening where the total stress range is equal to twice the yield strength; thus including the Bauschinger effect. Inclusion of the Bauschinger effect allows prediction of cyclic ratcheting. The Von Mises yield criterion and associative flow rule (Prandtl-Reuss equations) determined yielding due to the triaxial stress-state and the subsequent plastic strain components.

Elastic plastic stress strain data was obtained from the Haynes data and Catalytica testing at Metals Technology, Inc.[1] and is summarized in Table 4.2.1. Note that continuous curves were

available from the Metals Tech testing so these were used to create the shape of the stress strain curves with the Haynes data validating the yield strength.

	Haynes Manufacturer Data			Metals Tech Data				
Temp (F)	Modulus (106 psi)	0.2% Yield (psi)	Strain at .2% (in/in)	Modulus (106 psi)	0.02% Yield (psi)	Strain at .02% (in/in)	0.2% Yield (psi)	Strain at .2% (in/in)
70	31.6	87600	0.0048	34	61200	0.002	76000	0.0043
1000	25.3	78900	0.0051					
1200	23.9	81800	0.0054					
1292				20	70200	0.0036	77000	0.0058
1400	22.3	78800	0.0055					
1600	20.2	45000	0.0042					
1652				14	36600	0.0028	36800	0.0046
1800	19	7800	0.0024					
1832				8	9300	0.0013	10100	0.0032

Table 4.2.1 -- Stress Strain Data for Plasticity Model

The elastic plastic multilinear stress strain curves as used in the computations are shown in Figure 4.2.1. Metal temperatures between input curves are linearly interpolated.

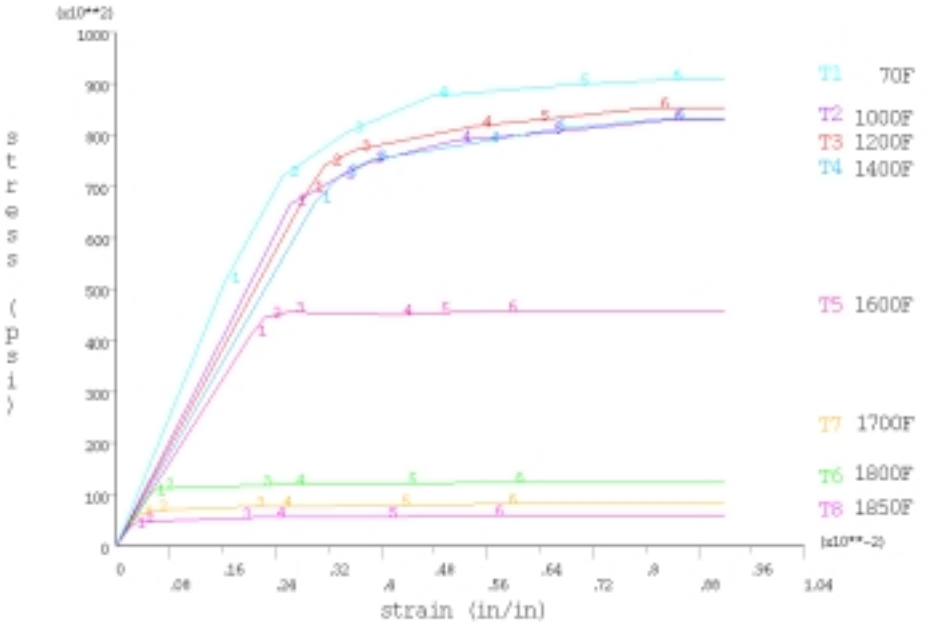

Figure 4.2.1 -- Multilinear stress strain curve for Haynes 214. Numbers on each curve indicate the end point of piecewise linear curves.

4.3 Creep and Stress Relaxation

Experimentally derived creep data were fit to an equation for input into the stress analyses. The creep constitutive equation is a function of stress, time and temperature. Primary creep regime is represented by the equation:

$$\partial\varepsilon/\partial t = C_1 \sigma^{C_2} t^{C_3} e^{-C_4/T} \quad (1)$$

Secondary creep regime is modeled as:

$$\partial\varepsilon/\partial t = C_7 \sigma^{C_8} e^{-C_{10}/T} \quad (2)$$

where: ε = equivalent creep strain (in/in)

σ = equivalent stress (psi)

t = time at end of substep (hours)

T = Metal temperature (°R)

C_1, C_2, C_3, C_4 = Primary creep material constants

C_7, C_8, C_{10} = Secondary creep material constants

Total creep strain is the sum of the primary and secondary creep. It is quite unreasonable to expect this equation to accurately predict creep over a wide range of stress, temperature and time. A better approach is to first understand the specific operating stress, temperature and time, then fit the equation according to these conditions. It will later be shown that the stress causing creep is between 500 and 1100 psi, the temperature is 1700°F and the operating time is up to 10,000 hours. There are variations in stress and temperature about these conditions so the constitutive equation should be checked nearby.

Initially, data from Haynes [Appendix B] were fit in order to develop the analytical method and begin to understand the importance of yielding versus creep, mechanical versus thermal load and load cycling. As has been described, properties more specific to the BMM were not obtained due to difficulty with the material creep testing. Results of the stress analyses with the Haynes data along with the limited foil creep testing provided enough insight into the behavior to determine future efforts on catalyst axial supports.

The process for fitting the creep constitutive equation to the Haynes creep data was as follows.

i) First, because the available data was at higher stress and shorter time than required, use was made of the Larson Miller time- temperature parameter:

$T (LM + \log t) =$ constant for a given stress

where: T = temperature (°R)

t = time (hours)

LM = material constant

This time temperature parameter was considered much more accurate than an extrapolation of the higher stress data at 1700°F to the actual operating stress.

ii) Data at 1700°F was between 1.8 (10,000 hrs) and 8.3 ksi (10 hrs), at 1800°F the creep data was at 0.57 (10,000 hrs) to 2.3 ksi (10 hrs) and at 1900°F the range of stress is 0.24 (10,000 hrs) to 1.4 ksi (10 hrs). Then to obtain the Larson Miller material constant for 1 ksi stress, 1900 to 1800°F data was utilized since the stress was contained within both data sets. At 1900°F, 1 ksi gives 1% creep strain in 45 hours (interpolation between stresses required). With a Larson Miller parameter of 27, the calculated 1800°F time to 1% strain is 840 hours. This exactly matches the measured time to 1% creep at 1800°F and 1 ksi.

iii) The Larson Miller parameter was applied to the 1800°F data to generate longer time data at 1700°F, which became the base data for fitting the creep equation. Note that this 100°F temperature difference causes a 20 times change in the number of hours to achieve a given creep strain.

iv) A power law curve was then fit to the creep strain versus time data to obtain the time exponent, C_3.

v) To find the stress constants, C_2 and C_8, a power law was fit to stress versus creep strain for short time and 8000 hours at 1700°F.

vi) The exponents on temperature, C_4 and C_{10}, were estimated by solving, using 1% creep strain data at 1700 and 1800°F:

$$\sigma_1{}^{C} i\, e^{-C/T_1} = \sigma_2{}^{C} i\, e^{-C/T_2}$$

vii) Finally, the constants C_1 and C_7 were solved to fit the data well at short and long times for the combined creep equation. At this point, constants were adjusted by trial and error to improve the match to the experimental data.

The creep constitutive equation constants are given in Table 4.3.1 and the comparison to measured creep data is shown in Table 4.3.2. At 1700°F, the equation matches especially well at the longer time. Across a range of stress and time at 1800°F, the equation gives excellent agreement to measured data.

Constant	Value
Primary C_1=	2.50E+14
Stress C_2=	9.20E-01
Time C_3=	-0.95
T_{metal} C_4=	1.10E+05
Secondary C_7=	2.00E-11
Stress C_8=	4
T_{metal} C_{10}=	3.50E+04

Table 4.3.1 -- Creep Constants

Time (hr)	Temp (F)	Stress (psi)	Total creep (in/in)	Primary (in/in)	Secondary (in/in)	Measured (in/in)
239	1700	1300	0.0016	0.0004	0.0013	0.001
473	1700	1300	0.0029	0.0004	0.0025	0.002
1110	1700	1300	0.0062	0.0004	0.0058	0.005
2017	1700	1300	0.011	0.0004	0.0106	0.01
3693	1700	1300	0.0198	0.0004	0.0194	0.02
10	1800	2100	0.0054	0.0046	0.0007	0.005
100	1800	1300	0.0044	0.0034	0.0011	0.005
1000	1800	870	0.0048	0.0026	0.0022	0.005
10000	1800	570	0.0059	0.002	0.004	0.005

Table 4.3.2 -- Comparison of Equation to Measured Creep Strain

It is important to note at this point that the creep data upon which these predictions are based shows some discrepancy. For example, the brochure data [Appendix B] lists 4.7 ksi to 0.5% creep in 100 hours whereas the creep results gives 0.5% creep due to only 59 hours and 4.0 ksi, both points at 1700°F. Clearly, this shows the degree of uncertainty in the actual material performance. However, by approximating a material model and performing the nonlinear structural analysis, significant qualitative understanding is gained and quantitative comparisons can be established. For instance, once a structural deformation rate is calculated for a certain material creep rate, estimates of deformation for other material creep rates or temperature changes can easily be made. Qualitatively, the effects of plasticity relative to creep, and thermal compared to mechanical load will be sought.

The finite element analysis computes changes in creep strain for finite time increments referred to as substeps. Therefore, the above equations are integrated over the substep and the creep strain increment computed. These substeps must be sufficiently small to allow redistribution of stress as yielding and creep occurs. After each substep, the strain increments are summed with the previous strain state and the geometry and stress state is updated. Again, the Von Mises yield criterion relates the triaxial stress-state to the creep equation stress and the associative flow rule (Prandtl-Reuss equations) determines the subsequent strain components.

V. Finite Element Model

5.1 Finite Element Mesh

The finite element mesh is shown in Figure 5.1.1. The model is constructed of predominately 8-noded hexahedral elements for accuracy with high computational efficiency. The large aspect ratio of the honeycomb geometry due to the thin foil relative to the BMM diameter and height, along with the minimum cyclic symmetry of a quarter sector results in a large number of elements. This model contains 158,484 elements and 319,700 nodes. Several meshes were analyzed to arrive at this construction, which obtains optimal accuracy with the minimum number of elements.

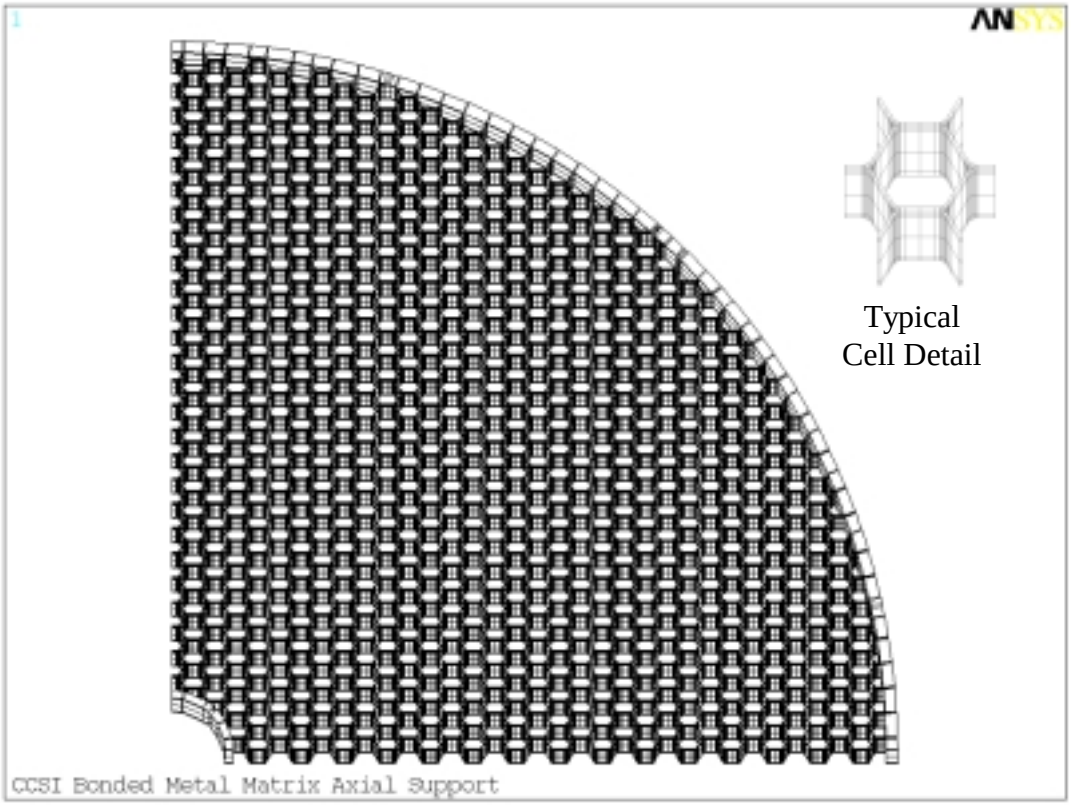

Figure 5.1.1 -- Finite Element Model

Brazing of the corrugated foils to construct the honeycomb creates radii at the joints between foil pairs. This radius was measured on numerous joints and found to be about 0.020 inches. In addition, the finite element analysis was run with 0.005 inch larger and smaller radii and found to not significantly affect the stress.

5.2 Loading

The metal temperature distribution applied to the thermal stress analyses was obtained from infrared imaging of the catalyst module during turbine operation at Silicon Valley Power. These temperatures are shown in Figure 5.2.1.

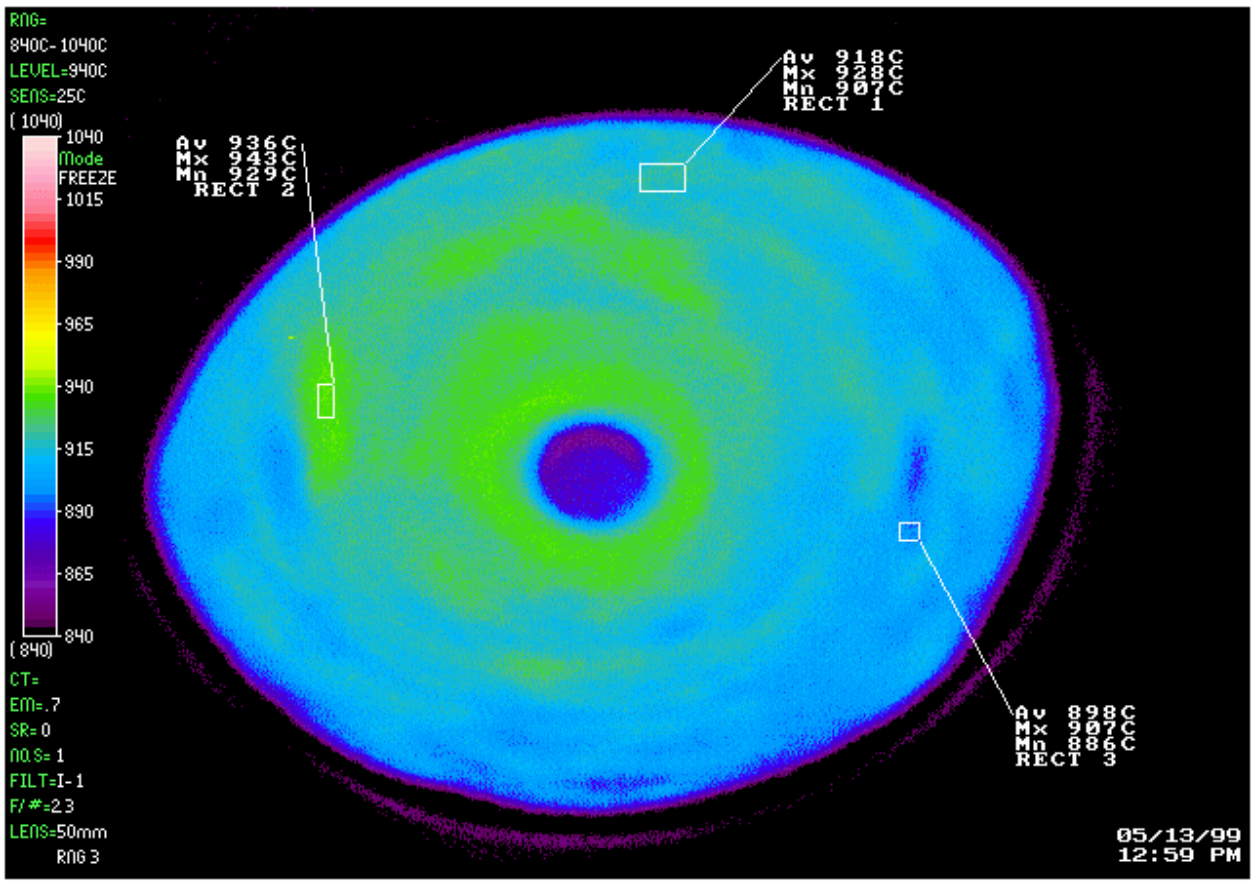

Figure 5.2.1 -- Metal Temperature Distribution Measured During Turbine Operation

Mechanical loading on the axial support is due to edge contact from the catalyst foils, which sustain a fluid pressure loss. Uniform pressure rather than discrete foil contacts were used to represent this edge load. Because the contacts are at most 0.040 inches apart, this approximation is considered reasonable. The pressure drop across the entire cross section used in these analyses was 1.0 psi and the uniform pressure load on the honeycomb edge was then 7.8 psi.

5.3 Boundary Conditions

Symmetry restraint conditions are applied at each cut boundary on the inner and outer diameters. Axial restraint is applied at the outer and inner diameter to represent the contact conditions within the assembled catalyst module.

VI. Finite Element Analysis Results

6.1 Quarter Sector Elastic Finite Element Analysis Results

The metal temperatures applied to the model are shown in Figure 6.1.1. This is an approximation of the previously shown measurements, which matches the hottest radial line and assumes that distribution over the quarter sector. This is considered fairly accurate though a slightly conservative loading for the stress analysis. Assuming the worst radial gradient exists all

around will produce slightly higher stress than the actual condition with a less severe gradient in most circumferential locations.

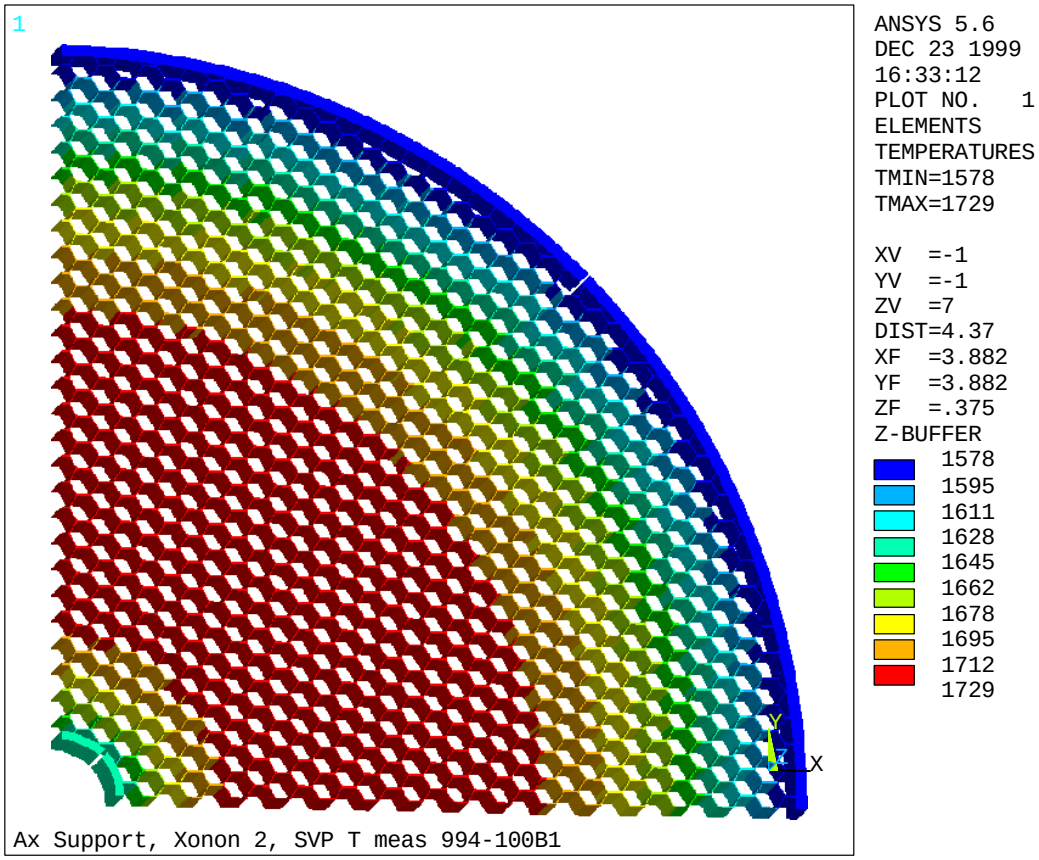

Figure 6.1.1 -- Heat Transfer Analysis Metal Temperature Distribution

6.2 Thermal Stress Results and Fatigue Limiting Location

Stress due to the thermal gradients and mechanical loading determines the number of load cycles necessary to cause low cycle fatigue. Equivalent stress due to the thermal and pressure load is show in the Figure 6.2.1 contour plot of the entire structure. Stress is highest near the thermal expansion slots in the inner and outer bands. A typical stress state in honeycomb cells within the sector is shown in Figure 6.2.2. These cells are near midspan along the lower edge of the previous figure. In general, this midspan region is critical for the long-term deformation of the entire structure. Equivalent stress throughout the BMM is also depicted more vividly in the bar graph in Figure 6.2.3. This graph summarizes the maximum stress versus radial location within three 30-degree slices of the 90-degree sector. The maximum stress is in the center slice at the outer diameter, adjacent to the thermal expansion slot and is the likely location of initial low cycle fatigue.

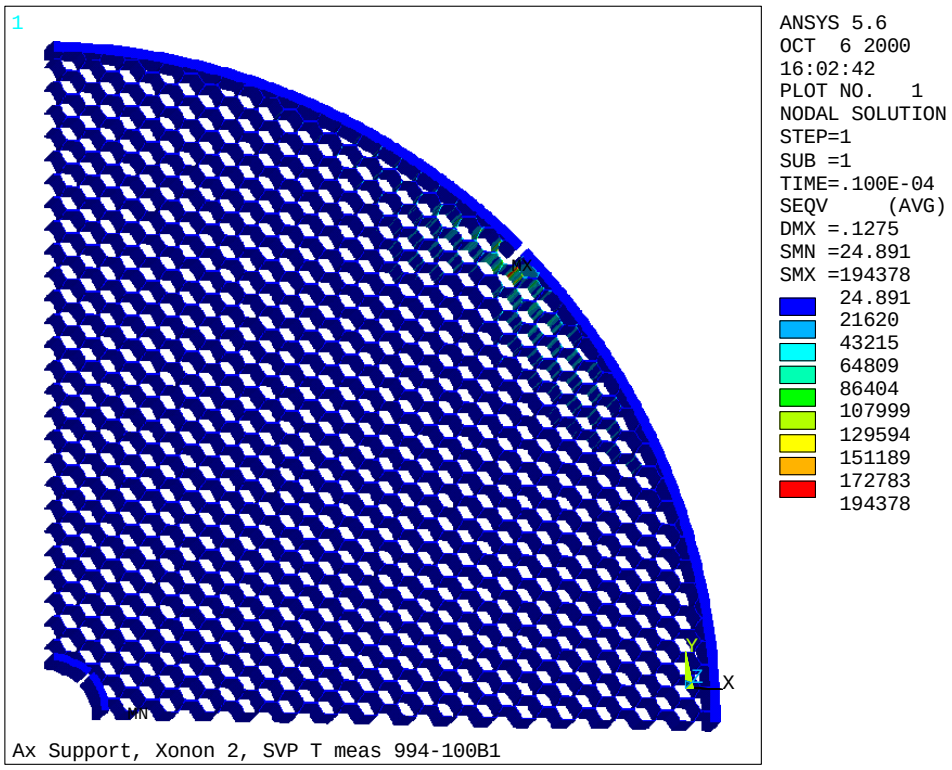

Figure 6.2.1 -- Equivalent Stress Due to Thermal and Pressure Load

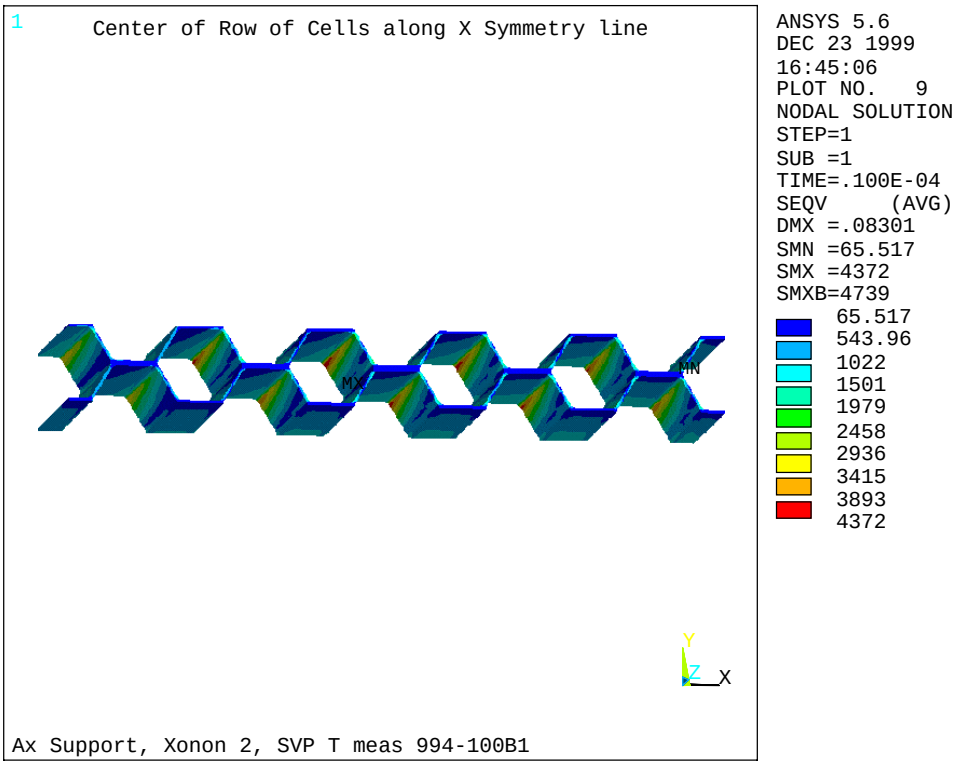

Figure 6.2.2 -- Equivalent Stress in Selected Elements at Midpsan.

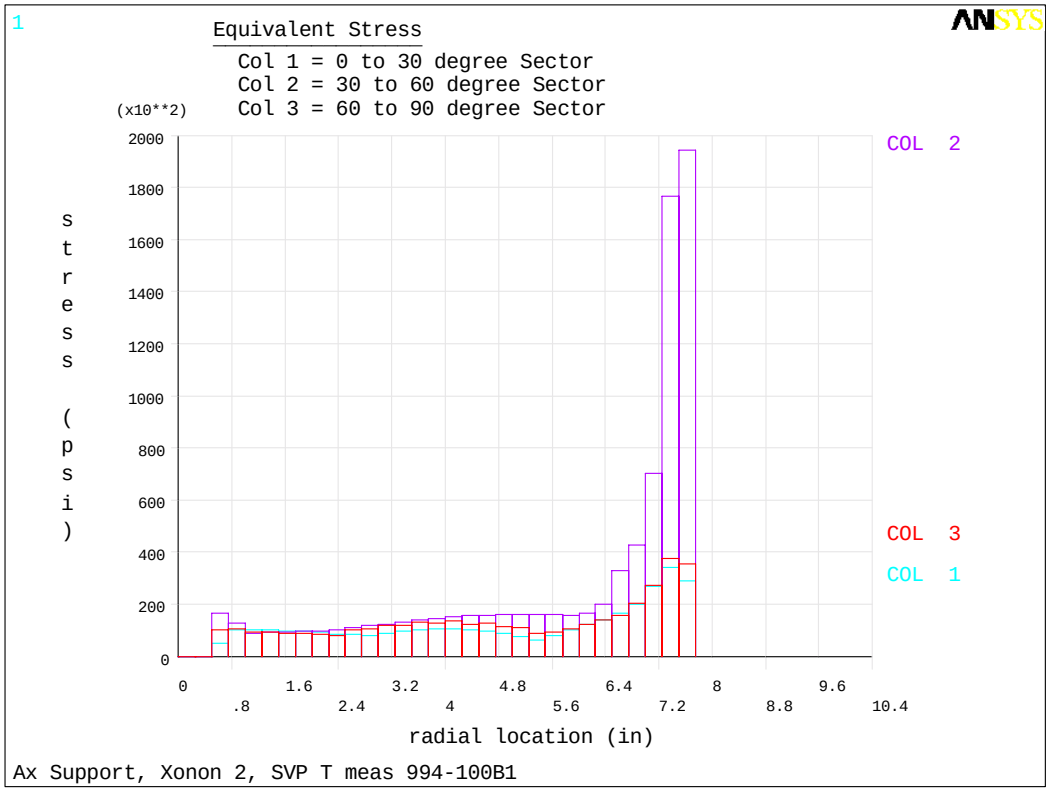

Figure 6.2.3 – Maximum Equivalent Stress at Radial Location within Each 30° Sector

6.3 Low Cycle Fatigue Prediction

A detailed view of the stress distribution near the expansion slot in the outer diameter ring is shown in Figure 6.3.1. Using the previously reported fatigue data for pretreated H214 at 900°C and 194 ksi, the number of cycles to fatigue failure is predicted to be less than 50. Fatigue cracks have been observed in actual engine hardware at this location after more than 50 starts. However, this condition does not cause a durability concern because the structural integrity is not compromised when a single or even multiple cell walls have separated near the thermal expansion slots. These cracks would need to extend along a significant portion of the outer ring to cause lack of support for the catalyst. If the initial cell wall fatigues in 50 cycles, then the adjacent cells acquire additional strain and fatigue (though at slightly lower rates), well over 600 cycles are required to connect between the expansion slots. This is very conservative since the more cells crack, the lower the fatigue stress becomes. The only other possibility, though even less likely, is that a section of honeycomb becomes liberated as cracks form a closed loop. There is insufficient stress away from the slot to cause this event.

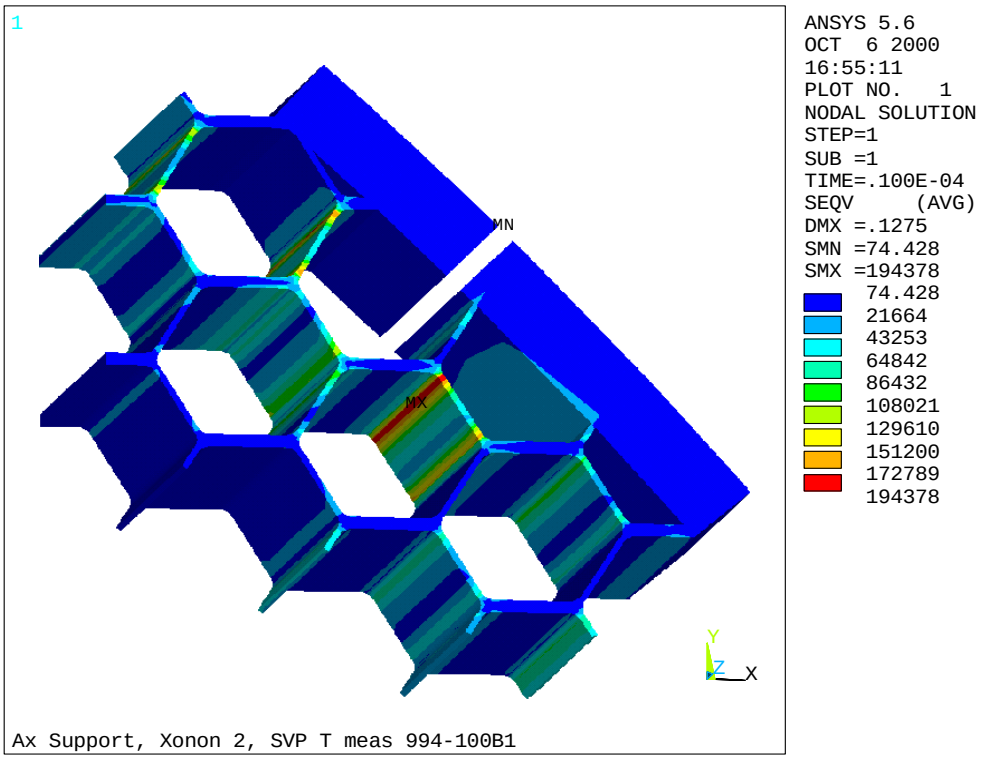

Figure 6.3.1 -- Equivalent Stress Near Outer Diameter Thermal Expansion Slot.

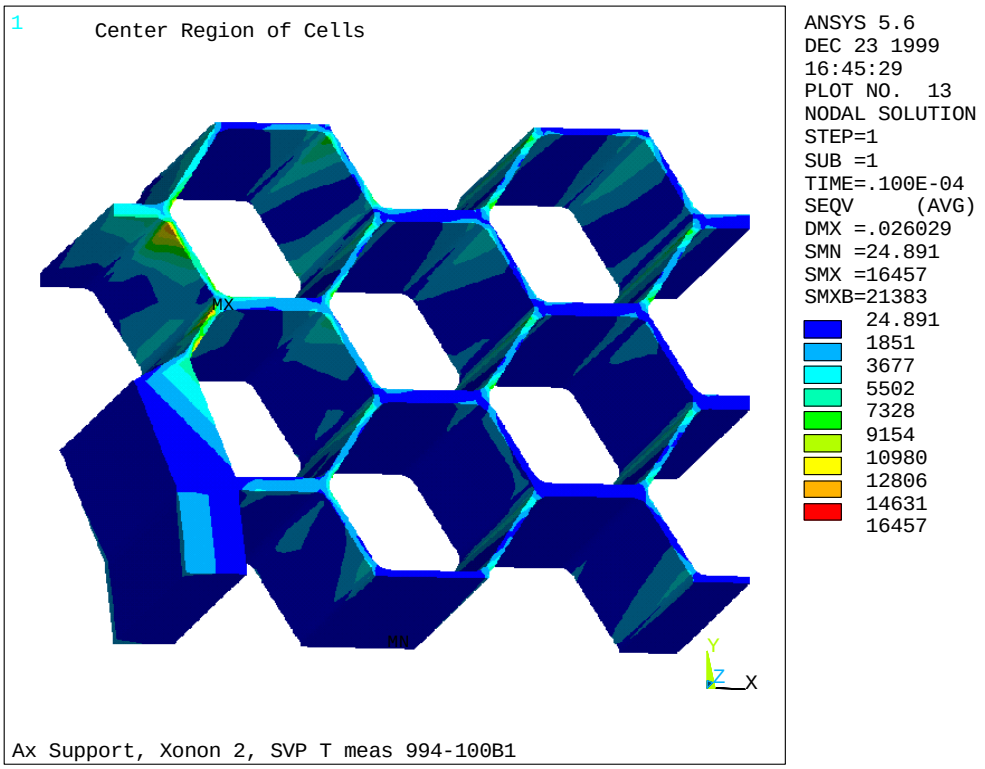

Figure 6.3.2 -- Equivalent Stress Near Inner Diameter Thermal Expansion Slot

A similar situation at the inner diameter, thermal expansion slots could pose a durability issue since far fewer structural connections between the foil and the support ring exist. Figure 6.3.2 shows the stress near this slot. Fortunately, extrapolating the fatigue data for pretreated H214 at 900°C and 16 ksi, the number of cycles to fatigue failure is predicted to be greater than 3000.

6.4 Pressure Load Only

Stresses resulting from pressure loading can only result in the deformation of the structure over time. Thermal stresses relax in short time whereas pressure load continues to drive movement for the entire operating time. Equivalent stress is summarized throughout the structure in Figure 6.4.1. Again the peak values occur near the expansion slots. Equivalent stress at midspan where most of the creep strain will accumulate and therefore indicates how the honeycomb will deflect over time is shown in Figure 6.4.2 with further detail shown in Figure 6.4.3.

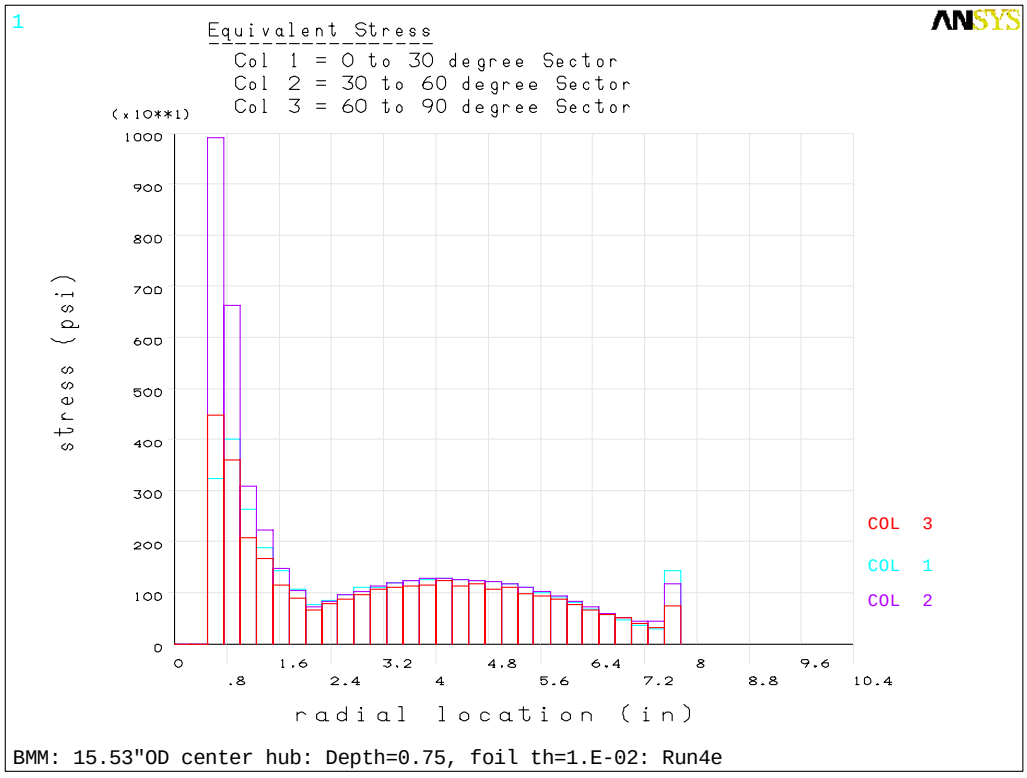

Figure 6.4.1 -- Pressure Load Only: Maximum Equivalent Stress at Radial Location within Each 30° Sector

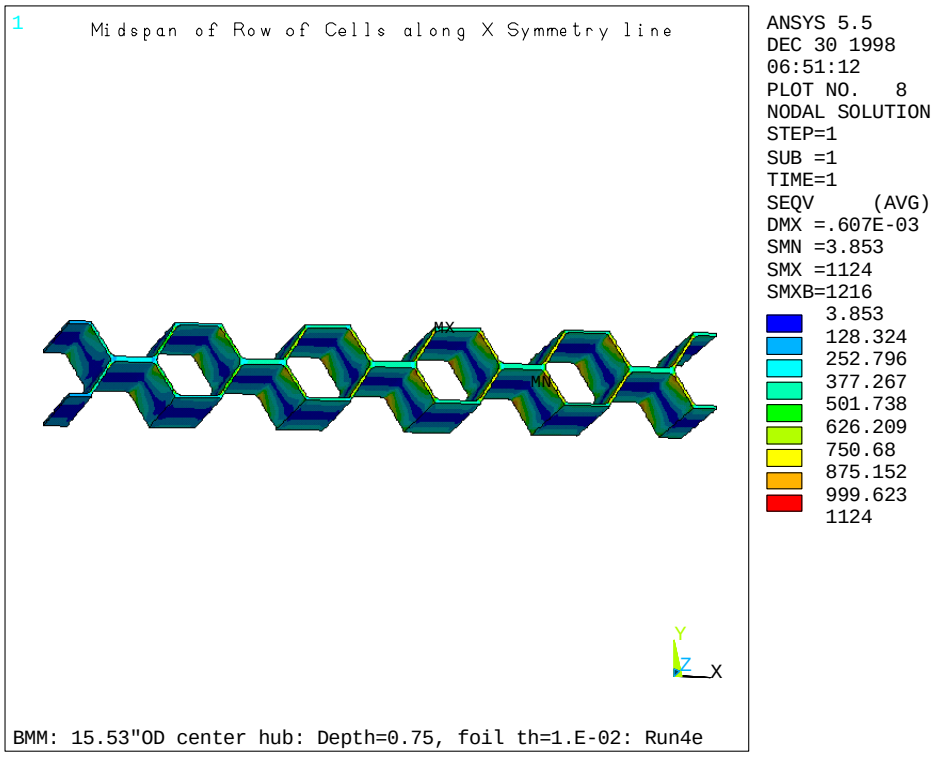

Figure 6.4.2 -- Equivalent Stress for Preesure Load in Selected Elements at Midpsan

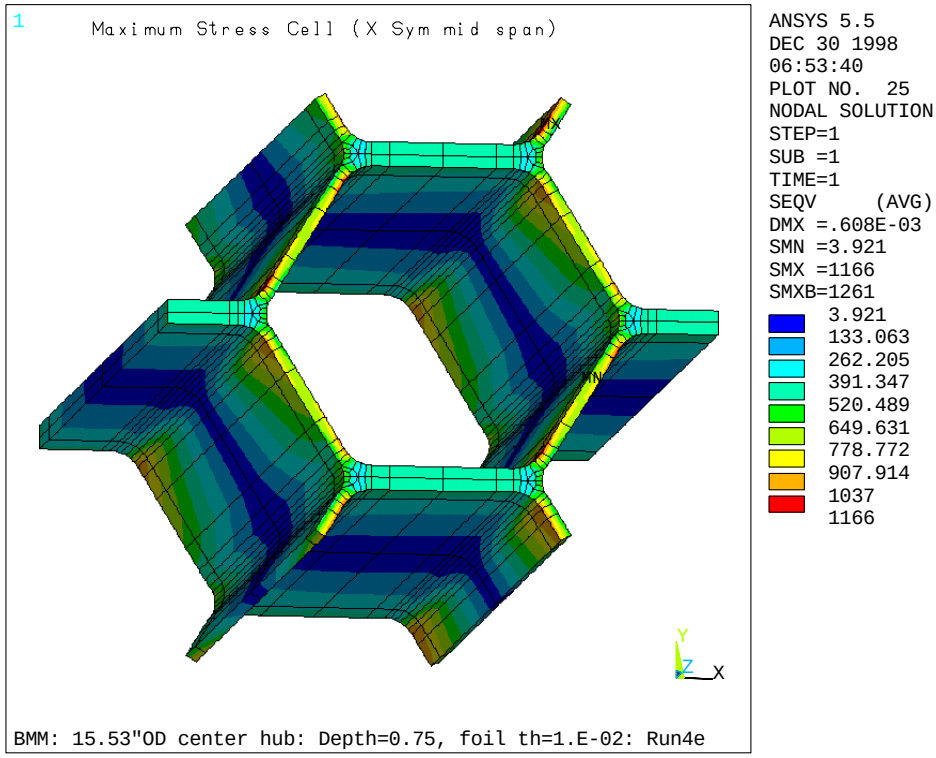

Figure 6.4.3 -- Detail of Single Cell Equivalent Stress at Midspan

No attempt will be made to explain the estimation of creep deformation from these results. Clearly, stresses and temperatures are high enough to cause creep deformation. The estimation of creep was completed but more importantly, the results of this section revealed unforeseen complications in this prediction that will now be addressed.

The combined effect of thermal stress exceeding yield and mechanical stress high enough to drive creep can also cause cyclic ratcheting[2]. Ratcheting causes additional deflection due to load-and-unload cycles. It is possible for this ratcheting of the deflection to continue indefinitely or to 'shakedown' and stop once the strain-state has reached a certain condition. The results of this section revealed the importance of including load cycling and plasticity in addition to creep in the prediction of permanent deflection. This significantly complicates this analysis.

6.5 One Row Elasto-Plastic Creep Finite Element Analysis

Addition of numerous loading cycles with the resulting reverse yielding caused the quarter sector model to be too large to analyze in a reasonable period of time. One iteration of the quarter sector finite element structural analysis required 1.7 CPU hours on a high performance engineering workstation (one 600 MHz Alpha processor with 1Gb of RAM running UNIX). The nonlinear analysis was expected to require 300 iterations to apply the loads, 400 iterations to creep for 200 hours and 300 iterations to unload. Therefore, 1000 hours of combustor simulation with 5 load cycles would require 4000 iterations or 6800 CPU hours. Obviously, a method of reducing the run time was needed.

6.5.1 Reduced Run Time Model

Because the results appear quite axisymmetric except for the expansion slot regions reducing the sector size was the best approach for increasing speed. Note that the local stress concentrations around the expansion slots are insignificant to the overall permanent deformation. After several elastic analyses of various reduced sectors and edge boundary conditions, it was found that a single row of cells with an axisymmetric edge restraint produced very accurate results. This model, refered to as the 'one row' model is compared to the quarter sector model in Table 6.5.1.1 for linear elastic behavior. Note that this comparison was completed for a BMM without a center ring and unsupported at the center, which has been used in testing. This configuration was considered the most difficult to approximate with a smaller sector so was used to develop the reduced model.

The equivalent stress remains within 20% of the large model, which is most important for determining yielding and creep. This was considered acceptable since this stage of the work was to understand relative significance of plasticity, creep and load cycling. Component stresses were less comparable but continued to have similar relative values, which is most important for the strain distribution using the associative flow rule. It was concluded that this model was acceptable for reducing run time for preliminary nonlinear analyses. Based on the results, a decision would be made regarding analyzing the larger model.

	Quarter Sector	One Row
Pressure & Thermal Load		
Axial Displacement (in)	0.022	0.0212
σeq (ksi) quarter span	10.9	10.7
σx	-3.8 / 1.3	-3.8 / 1.3
σy	-8.4 / 2.9	-8.4 / 2.9
σz	-2 / 1.5	-2 / 1.5
σeq center span	7.3	5.1
Pressure Load Only		
Axial Displacement (in)	0.0092	0.0047
σeq (ksi) quarter span	3.6	3
σx	-1.9 / 1.9	-1.3 / 1.3
σy	-3.6 / 3.6	-2.6 / 2.6
σz	-0.4 / 0.4	-0.4 / 0.4
σeq center span	4.2	2.6

Table 6.5.1.1 -- Comparison of Full to Reduced Size Model

6.5.2 Elasto-Plastic Creep Results

A nonlinear FE analysis of the one row model with the inclusion of plasticity and creep material behavior was completed. Loading was applied as a linear ramp over 72 seconds similar to how the turbine is started. This was done gradually in 50 steps in order to allow plastic deformation to redistribute. Next, the load was held constant for 200 hours while creep strain accumulated.

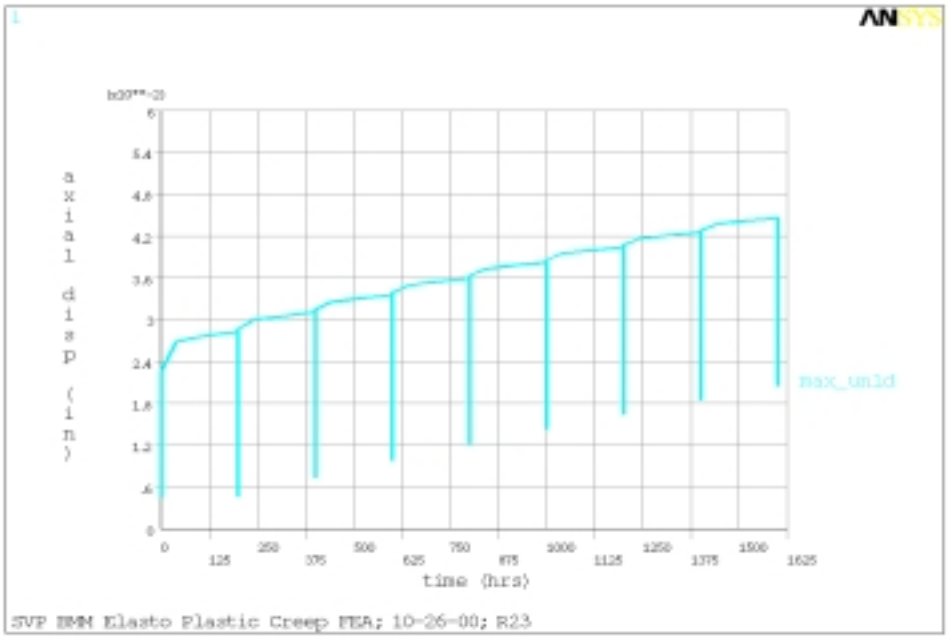

Figure 6.5.2.1 -- Axial deformation versus time for the One Row FE Elasto-Plastic-Creep Analysis.

The load was removed analogous to the load application method. This cycle was repeated 8 times.

Axial deformation versus time results provide the most evidence for evaluating axial support creep damage and can be easily compared to field measurements. Computed axial deformation versus time is plotted in Figure 6.5.2.1 near the mid-span between the inner and outer rings. At each 200 hour increment, the deflection appears to step change due to the relatively short time required to remove and apply load. Also, note that the results appear to be step-wise linear rather than continuous. This occurs because results at discete times are stored in the solution to reduce use of computer disk space. After 1600 hours the FE analysis computes .020 inches of permanent axial deformation. Each 200 hour increment increases the deflection by .0022 inches.

The deflected shape with color contours of axial deflection under full load and at shut down after 1600 hours are shown in Figure 6.5.2.2. The maximum deflection corresponds to the results plotted in the previous figure and occurs near the middle of the span.

Total, elastic, plastic and creep equivalent strain contours are given in Figure 6.5.2.3 and 6.5.2.4 for a representative honeycomb cell near midspan at full load. The largest strains occur at the joints between foils and are caused by bending of the foil.

Exaggerated deformation of this honeycomb cell is shown in Figure 6.5.2.5. This clearly shows that the deformation of the entire axial support is due to the local bending of the cell foils near the joints.

The maximum strains from the above honeycomb cell are plotted versus time in Figure 6.5.2.6. There is reversal of the plastic strain and subsequent change in the creep rate at each start up and shutdown. This will significantly increase the amount of deformation given load cycling during operation.

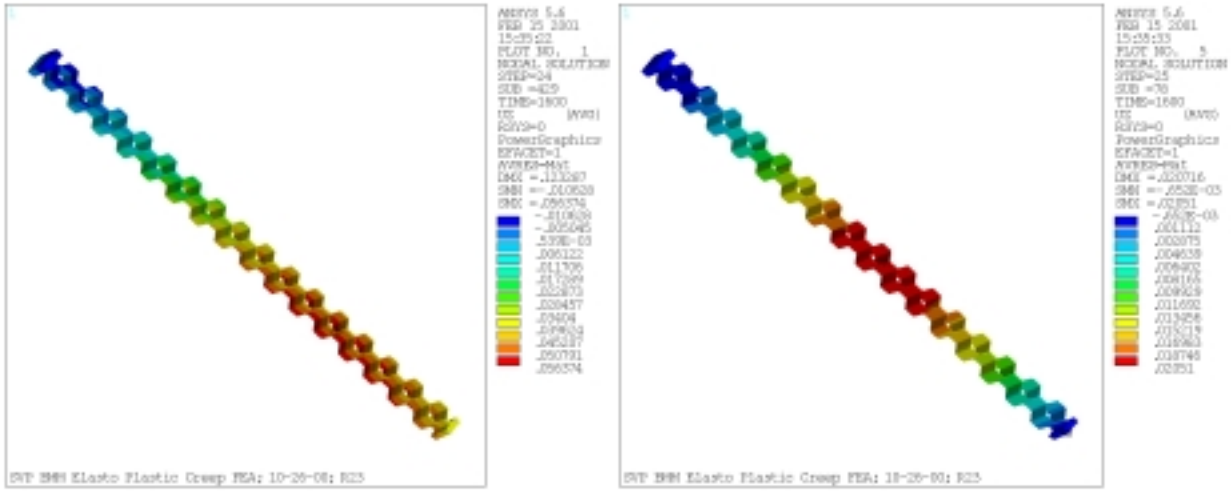

Figure 6.5.2.2 -- Axial deflection at full load (left) and shutdown (right)

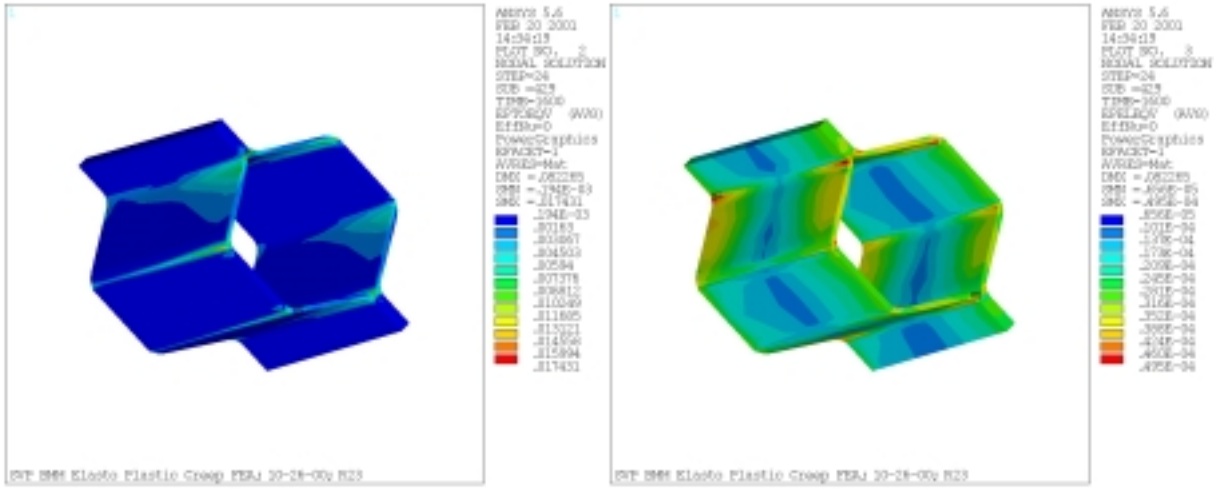

Figure 6.5.2.3 -- Total Strain (left) and Elastic Strain (right) for representative cell

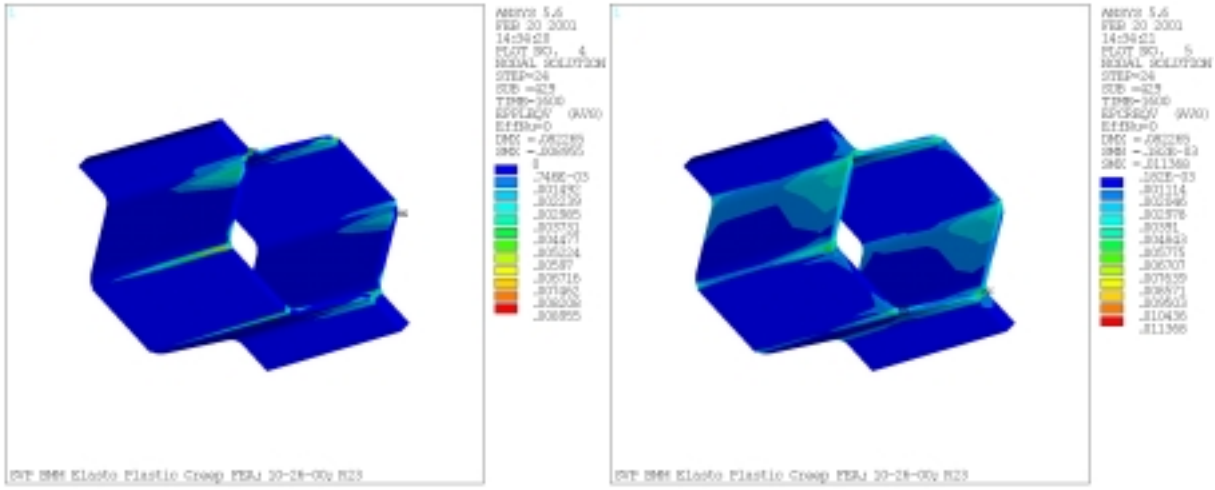

Figure 6.5.2.4 -- Plastic Strain (left) and Creep Strain (right) for representative cell

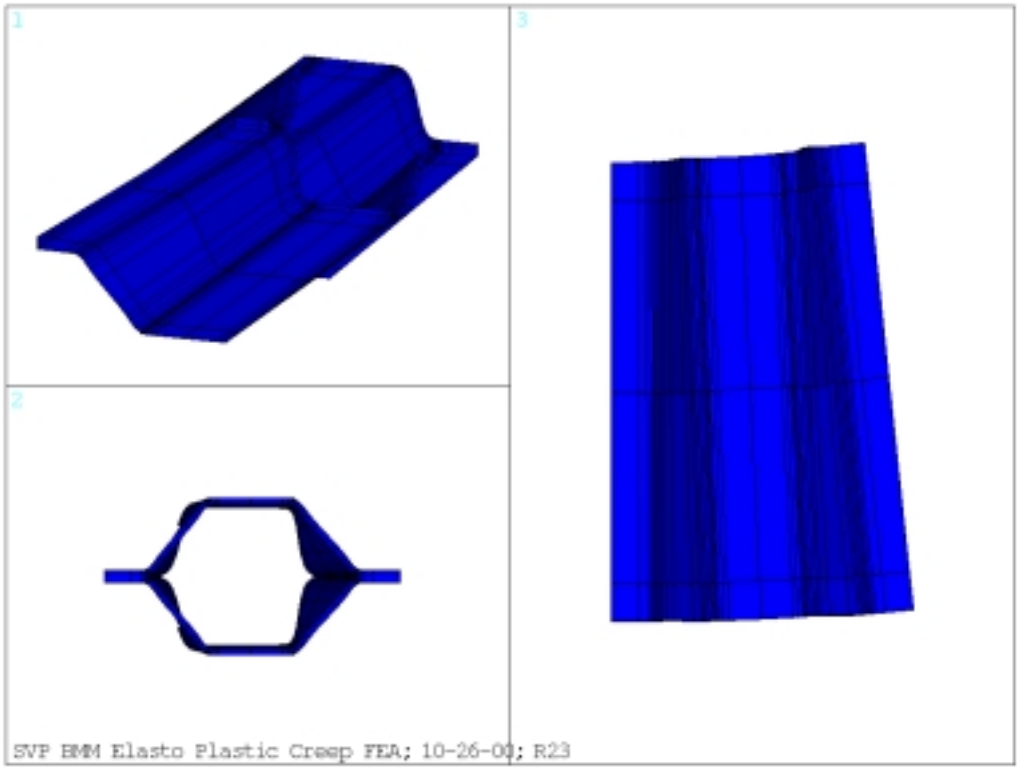

Figure 6.5.2.5 -- Deformed shape at full load after 1,600 hours

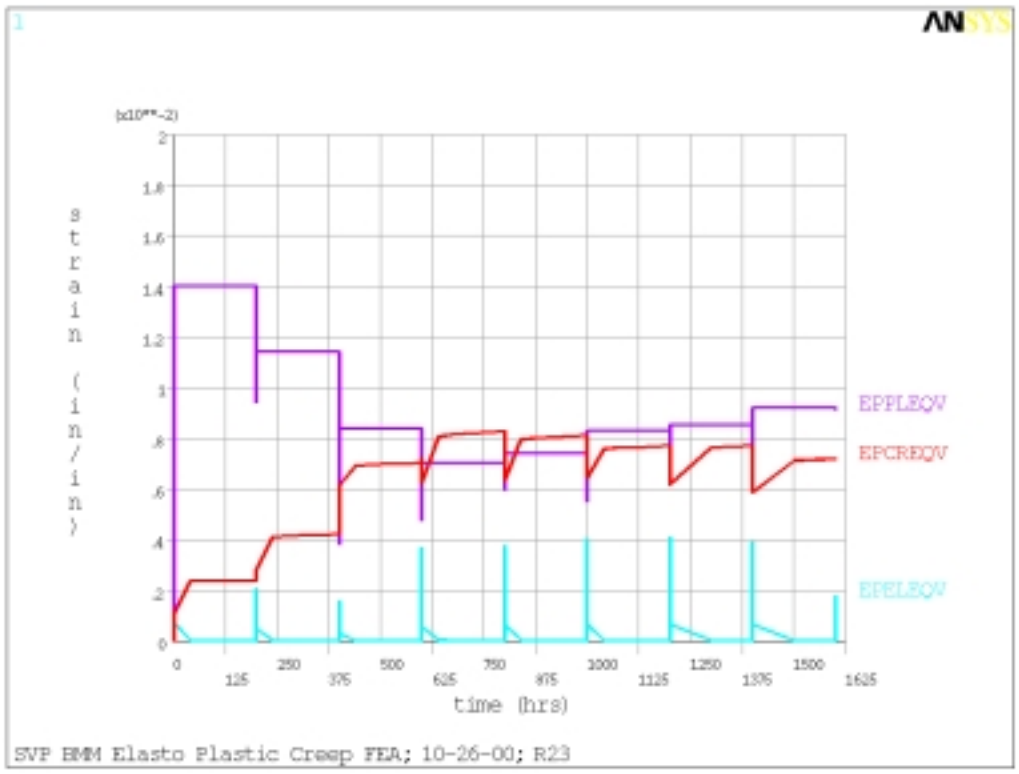

Figure 6.5.2.6 -- Maximum equivalent strains from previous cell versus time

6.5.3 Cyclic Ratcheting Significance

At each shutdown, the reversal of plasticity results in ratcheting of the deformation upon restarting. This deformation mechanism is considered very detrimental to most designs since deformation is added with each load cycle regardless of operating time[3]. As can be seen in the previous Figure 6.5.2.6, each start stop adds approximately 0.0003 inches of axial deflection compared to continuous operation without a stop. After fifty starts, there is an added 0.015 inches of permanent deflection which is considerable compared to the computed deformation. Not only is significant deflection added, but also the ability to predict the behavior is much more difficult because the material constitutive model must precisely represent the characteristics of the yield surface.

6.6 Comparison to Combustor Operation

6.6.1 Deformation versus Time at Silicon Valley Power (SVP)

Measurements of an operating Xonon combustion system at Silicon Valley Power were taken over 4129 hours of operation with approximately 50 starts. The maximum axial deflection, which occurs near midspan between the center and outer diameter is summarized in Table 6.6.1.1.

Time (hrs)	Axial Deflection (in)
0	0
1107	0.092
1408	0.107
2065	0.115
3056	0.126
3180	0.136
4129	0.154

Table 6.6.1.1-- SVP Deflection vs time

Extrapolating the analytical prediction to 4165 hours, assuming the deformation rates continue:

0.020	Computed deflection 1,600 hrs, 8 starts
+ (4165-1600)* (.0022 -.0003)/200	Creep rate minus ratcheting times added hours
+ (50-8)*.0003	Ratchet rate time added starts
0.057 inches	

The analytical prediction has underestimated the deformation seen in operation by 0.154/0.057 = 2.7 times. Several explanations for this shortcoming will be discussed.

6.6.2 Explanations for Under-Prediction

As discovered in the material creep testing, foil may have a considerably higher creep rate than that found in sheet material. For the honeycomb foil with as few as 3 grains through thickness,

creep resistance is weakened considerably and a 2.8 increase in creep rate was seen in short term testing. The material constitutive equation for this analytical prediction was based upon the more creep resistant sheet data. This difference alone would account for the under-prediction.

The material data upon which creep is represented in the computer simulation may not accurately describe the material for other reasons as well. None of the material data utilized to formulate the creep constitutive equation is based on test data for longer than 2,000 hours. Use has been made of time temperature extrapolation to model the material at longer time. This is notoriously inaccurate at these high temperatures where creep strength is deteriorating steeply. Also, the data is at higher stress rate, little is known about the behavior at lower stress.

Finally, the occurrence of ratcheting adds to the difficulty of representing the material with a set of equations. Not only is the elastic-plastic stress strain curve needed, but the shift of the yield surface, based on the Bauschinger effect, is also critical but difficult to measure.

VII. Conclusions/Recommendations

The mechanical durability of a combustion catalyst axial support has been investigated through material testing and computer simulation. Material testing was performed to obtain fatigue, creep and plasticity behavior. These material properties were input to a finite element structural analysis to gain valuable insight into the mechanical reliability of this device. Very good agreement with observed fatigue cracking was obtained.

The analysis was unable to predict the permanent deformations observed on actual hardware. Clearly, the leading cause of this discrepancy is the lack of good material data. Achieving more accurate permanent deformation predictions will require measuring creep strain of the actual foil thickness material at the stress levels experienced in the axial support.

References and Notes

[1] Metals Technology, Inc Certified Test Report No. 250450, 250451 and 250453, (10/13/98).
[2] Ratcheting ASME Boiler and Pressure Vessel Code Case N-47.
[3] ibid

Appendix A -- Creep results of foils done at MCL

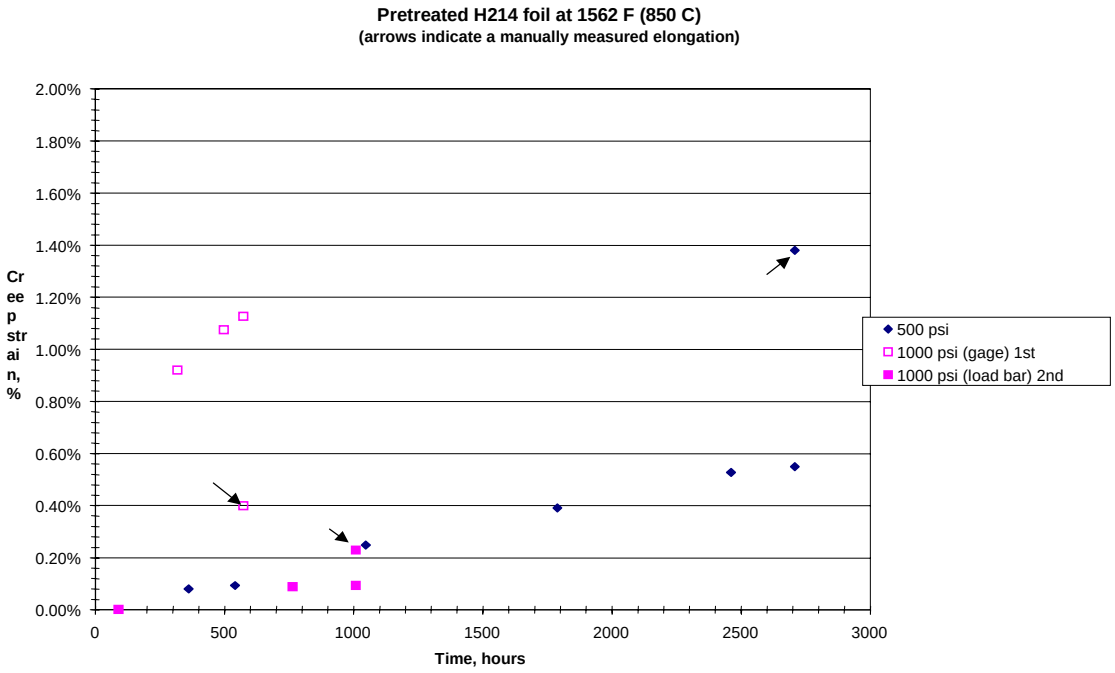

Figure A1 -- Pretreated H214 foil creep results at 1562F (850C)

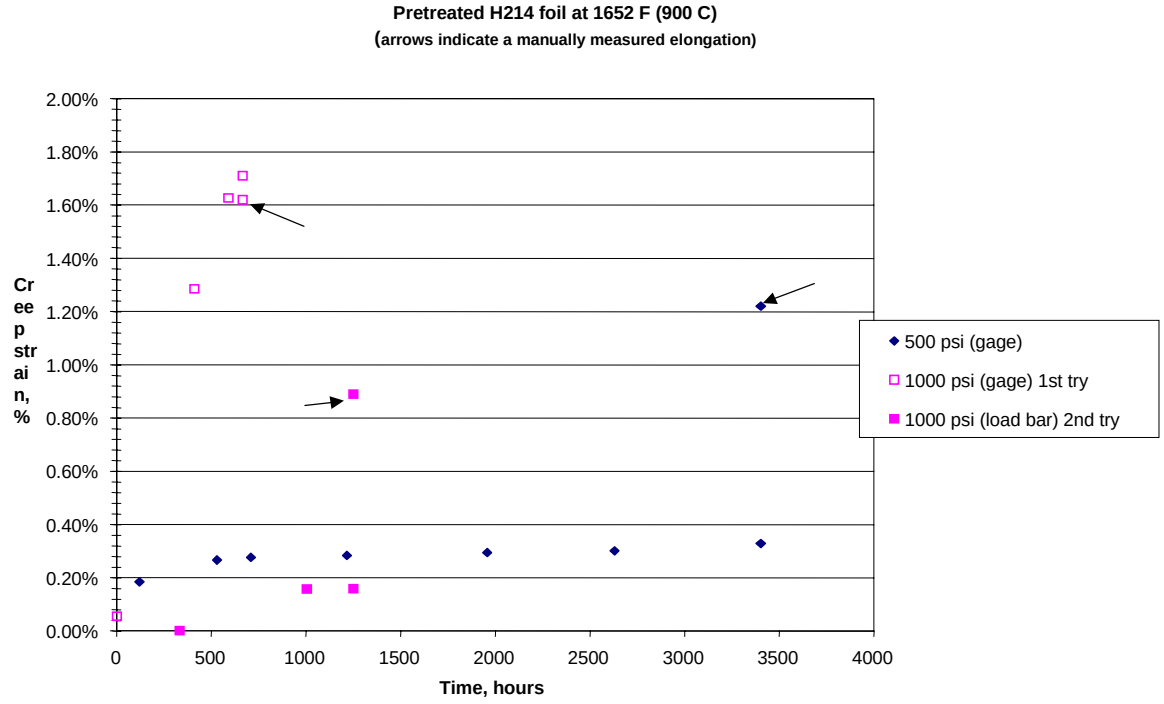

Figure A2 -- Pretreated H214 foil creep results at 1652F (900C)

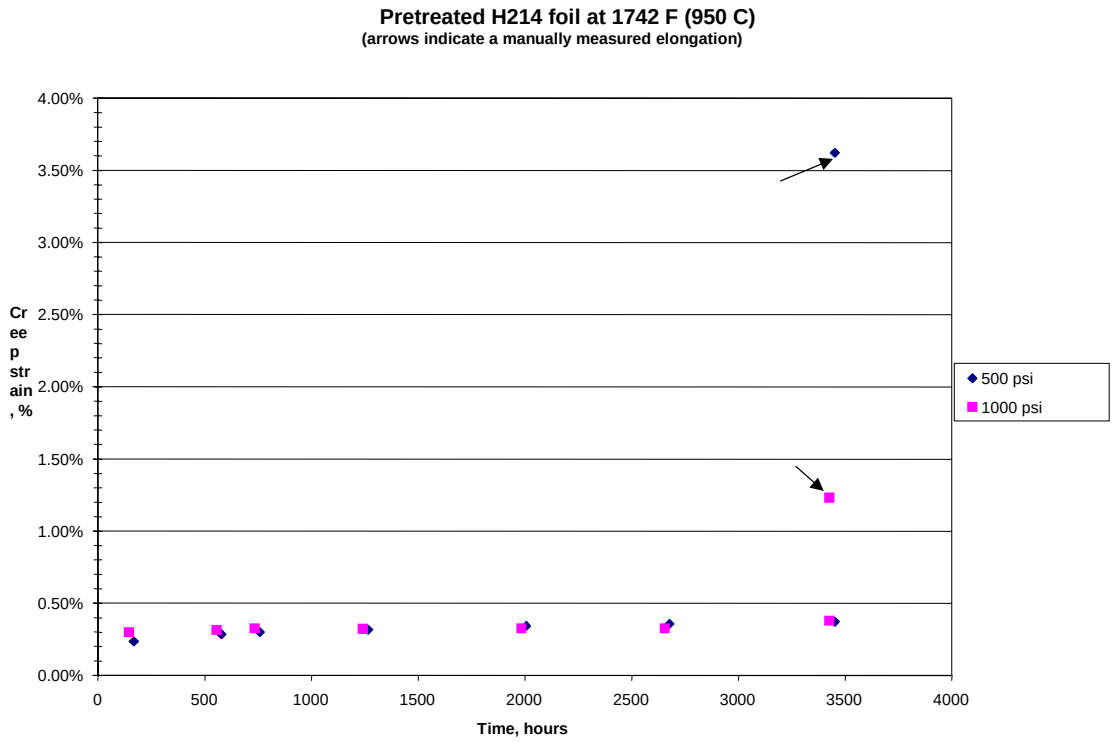

Figure A3 -- Pretreated H214 foil creep results at 1742F (950C)

Appendix B -- Haynes Material Property Data
(from Haynes International Web site http://www.haynesintl.com/214H3008C)

Temperature			Average Initial Stress, Ksi (MPa) to Produce Specified Creep and Rupture							
°F	°C	Creep, Percent	10 Hours		100 Hours		1,000 Hours		10,000 Hours*	
1400	760	0.5	37.2	(255)	27.5	(190)	20.4	(140)	15.1	(105)
		1.0	39.8	(275)	29.5	(205)	21.9	(150)	16.2	(110)
		Rupture	47.9	(330)	33.9	(235)	24.0	(165)	17.0	(115)
1500	815	0.5	23.4	(160)	17.4	(120)	12.9	(89)	9.6	(66)
		1.0	26.3	(180)	18.6	(130)	13.5	(93)	9.8	(68)
		Rupture	30.2	(210)	20.9	(145)	14.5	(100)	10.0	(69)
1600	870	0.5	13.8	(95)	9.6	(66)	6.5	(45)	4.3	(30)
		1.0	15.9	(110)	10.5	(72)	6.8	(47)	4.4	(30)
		Rupture	22.4	(155)	13.2	(91)	7.8	(54)	4.5	(31)
1700	925	0.5	7.6	(52)	4.7	(32)	2.9	(20)	1.8	(12)
		1.0	8.3	(57)	5.1	(35)	3.1	(21)	1.9	(13)
		Rupture	11.0	(76)	6.5	(45)	3.9	(27)	2.3	(16)
1800	980	0.5	2.1	(14)	1.3	(9.0)	0.87	(6.0)	0.57	(3.9)
		1.0	2.3	(16)	1.5	(10)	0.96	(6.6)	0.63	(4.3)
		Rupture	3.7	(26)	2.5	(17)	1.7	(12)	1.2	(8.3)
1900	1040	0.5	1.2	(8.3)	0.69	(4.8)	0.41	(2.8)	0.24	(1.7)
		1.0	1.4	(9.7)	0.84	(5.8)	0.50	(3.4)	0.30	(2.1)
		Rupture	3.2	(22)	2.0	(14)	1.2	(8.3)	0.76	(5.2)
2000	1095	0.5	0.72	(5.0)	0.41	(2.8)	0.24	(1.7)	0.14	(1.0)
		1.0	0.90	(6.2)	0.53	(3.7)	0.31	(2.1)	0.18	(1.2)
		Rupture	2.2	(15)	1.4	(9.7)	0.92	(6.3)	0.59	(4.1)

* Significant extrapolation for 0.5% and 1.0% creep values

TYPICAL TENSILE PROPERTIES

Cold-Rolled and Solution Annealed Sheet, 0.078 to 0.125 Inches (2.0 to 3.2 mm) Thick*

Test Temperature		Ultimate Tensile Strength		Yield Strength at 0.2% Offset		Elongation in 2 in. (50.8 mm)
°F	°C	Ksi	MPa	Ksi	MPa	%
Room	Room	144.2	995	87.6	605	36.8
1000	540	125.5	865	78.9	545	40.4
1200	650	118.5	815	81.1	565	25.5
1400	760	102.0	705	78.8	645	16.3
1600	870	58.2	400	45.0	310	15.4
1800	980	15.2	105	7.8	54	61.3
2000	1095	8.4	58	3.9	27	61.0
2100	1150	4.6	32	1.8	12	89.2
2200	1205	4.4	30	1.3	9	74.8

* Average of six tests for each condition

Hot-Rolled and Solution Annealed Plate, 0.500 Inches (12.7 mm) Thick*

Test Temperature		Ultimate Tensile Strength		Yield Strength at 0.2% Offset		Elongation in 2 in. (50.8 mm)
°F	°C	Ksi	MPa	Ksi	MPa	%
Room	Room	138.9	960	82.2	565	42.8
1000	540	120.0	825	71.5	495	47.8
1200	650	114.9	790	75.9	525	33.0
1400	760	97.4	670	73.6	505	23.1
1600	870	66.4	460	50.4	345	33.6
1800	980	16.7	115	8.4	58	86.4
2000	1095	9.0	62	4.2	29	88.6
2100	1150	6.6	46	2.1	14	99.4
2200	1205	5.0	34	1.4	10	91.5

* Average of six tests for each condition

DYNAMIC MODULUS OF ELASTICITY

Temp., °F	Dynamic Modulus of Elasticity, 10^6 psi	Temp., °C	Dynamic Modulus of Elasticity, GPa
Room	31.6 x 10^6 psi	Room	218 GPa
200	30.6 x 10^6 psi	100	210 GPa
400	29.6 x 10^6 psi	200	204 GPa
600	28.7 x 10^6 psi	300	199 GPa
800	27.4 x 10^6 psi	400	190 GPa
1000	25.3 x 10^6 psi	500	184 GPa
1200	23.9 x 10^6 psi	600	177 GPa
1400	22.3 x 10^6 psi	700	170 GPa
1600	20.2x 10^6 psi	800	162 GPa
1800	19.0 x 10^6 psi	900	151 GPa
		1000	137 GPa